J. Phys. B: At. Mol. Opt. Phys. **41** (2008) 175103 (11pp) doi:10.1088/0953-4075/41/17/175103

Investigation of the molecular conformations of ethanol using electron momentum spectroscopy

C G Ning[1], Z H Luo[1], Y R Huang[1], B Hajgató[2,3], F Morini[2], K Liu[1], S F Zhang[1], J K Deng[1] and M S Deleuze[2]

[1] Department of Physics and Key Laboratory of Atomic and Molecular NanoSciences of MOE, Tsinghua University, Beijing 100084, People's Republic of China ,
[2] Research Group of Theoretical Chemistry, Department SBG, Hasselt University, Agoralaan Gebouw D, B-3590 Diepenbeek, Belgium

E-mail: ningcg@tsinghua.edu.cn, djk-dmp@tsinghua.edu.cn and michael.deleuze@uhasselt.be

Received 20 May 2008, in final form 9 July 2008
Published 26 August 2008
Online at stacks.iop.org/JPhysB/41/175103

Abstract
The valence electronic structure and momentum-space electron density distributions of ethanol have been investigated with our newly constructed high-resolution electron momentum spectrometer. The measurements are compared to thermally averaged simulations based on Kohn–Sham (B3LYP) orbital densities as well as one-particle Green's function calculations of ionization spectra and Dyson orbital densities, assuming Boltzmann's statistical distribution of the molecular structure over the two energy minima defining the *anti* and *gauche* conformers. One-electron ionization energies and momentum distributions in the outer-valence region were found to be highly dependent upon the molecular conformation. Calculated momentum distributions indeed very sensitively reflect the distortions and topological changes that molecular orbitals undergo due to the internal rotation of the hydroxyl group, and thereby exhibit variations which can be traced experimentally. The B3LYP model Kohn–Sham orbital densities are overall in good agreement with the experimental distributions, and closely resemble benchmark ADC(3) Dyson orbital densities. Both approaches fail to quantitatively reproduce the experimental momentum distributions characterizing the highest occupied molecular orbital. Since electron momentum spectroscopy measurements at various electron impact energies indicate that the plane wave impulse approximation is valid, this discrepancy between theory and experiment is tentatively ascribed to thermal disorder, i.e. large-amplitude and thermally induced dynamical distortions of the molecular structure in the gas phase.

(Some figures in this article are in colour only in the electronic version)

1. Introduction

Ethanol is a molecule of great relevance in chemistry and astrophysics [1]. In its electronic ground state, ethanol exists in two stable conformations, namely the *anti* and the *gauche* structures that differ by the internal rotation of the hydroxyl group about the carbon–oxygen axis [2]. The *anti* conformer[4] was found to be 39.2 cm^{-1} slightly more stable

[3] Present address: General Chemistry Division, Free University of Brussels (VUB), Pleinlaan 2, B-1050 Brussels, Belgium.

[4] Conformers are also occasionally referred to as rotamers, or somewhat more ambiguously, as conformational isomers. See for instance the monumental treaty by [3] or any recent textbook on molecular structure theory. The various conformations that characterize a structurally versatile molecule correspond to energy minima that are separated by low energy barriers (a few kcal mol^{-1}, at most). Conformers therefore rapidly interconvert and cannot be physically isolated at room temperature. In contrast, structural isomers are molecular structures characterized by different chemical connections between atoms, and which relate to energy minima that are separated by huge energy barriers (>30 kcal mol^{-1}) corresponding to chemical reactions. True isomers can thus be isolated and display different physico-chemical properties.

than the *gauche* species, according to experiments employing microwave spectroscopy [4]. The problem of rotational isomerism of ethanol has been further extensively investigated by means of infrared spectroscopy [2, 5–8]. A recent carbon 1s synchrotron radiation spectroscopic study indicates that detailed pieces of information on the molecular conformation of ethanol are also amenable from the core ionization bands [9, 10]. The small size of this molecule enables high-level theoretical investigations of its potential energy surface. A study of interest is that by Senent *et al* [2], who explored in full details at the MP4(SDTQ) level [2] the conformational energy surface associated with the internal rotations of the hydroxyl and methyl groups [2]. The reader is referred in particular to a thorough study by Kahn and Bruice [11] of energy differences between the main stationary points on the potential energy surface of ethanol, using the principles of a focal point analysis (FPA) [12, 13].

Compared with the many investigation of the molecular structure of ethanol, detailed studies of the electronic structure of this compound are relatively scarce. Early works on the ionization properties of ethanol comprise the HeI ultraviolet photoemission spectroscopy (UPS) by Kimura *et al* [14], as well as the more extended HeII UPS measurements of Potts *et al* [15]. These works were restricted to an assignment of spectral bands on the ground of the *anti* conformation only, and did not account for the contribution of the *gauche* conformation.

In the present work, we report a comprehensive study of the valence electronic structure and wavefunction of ethanol and their interplay with the molecular architecture, according to experiments employing high-resolution electron momentum spectroscopy [16, 17] at various electron impact energies. In support of this investigation, the experimentally obtained electron binding energy spectrum is assigned against thorough calculations employing one-particle Green's function (or electron propagator) theory [18, 19] of the valence ionization spectrum that account for configuration interactions both in the initial and final states.

Electron momentum spectroscopy is known to be a powerful method for experimentally reconstructing valence orbital densities [16, 17, 20–25]. Previous studies combining EMS experiments with theoretical modelling have shown that with this powerful spectroscopic technique, it is also possible to experimentally study the influence of the molecular conformation onto the spread, shape and topology of molecular orbitals [26–32]. A difficulty that has led in the past to erroneous interpretations of EMS measurements on structurally versatile molecules is that the influence of the molecular conformation onto electron binding energies must absolutely be taken into account in the analysis [29].

2. Theory and experimental details

Electron momentum spectroscopy (EMS) is a binary (e, 2e) experiment in which an incident electron with high enough energy (E_0) induces ionization of a molecular target [16, 17, 33, 34]. The scattered and ionized electrons are subsequently detected in coincidence at equal kinetic energies and equal polar angles, i.e. $E_1 \approx E_2$, and $\theta_1 \approx \theta_2 \approx 45^\circ$, and therefore at equal momenta, $p_1 \approx p_2$. The initial momentum p of the knocked-out electron obeys therefore a simple conservation rule,

$$p = \{(2p_1 \cos\theta_1 - p_0)^2 + [2p_1 \sin\theta_1 \sin(\phi/2)]^2\}^{1/2}, \quad (1)$$

where p_0 is the momentum of the incident electron. Throughout this work, electron momenta are given in atomic units (1 au = 1 a_0^{-1}, with a_0 the Bohr radius, i.e. 0.529 18 Å).

Vertical ionization spectra are computed using one-particle Green's function (1p-GF) theory [18, 19] in conjunction with the so-called third-order algebraic diagrammatic construction scheme, ADC(3) [35]. At this level, the ionized states are described in terms of one-hole (1h) and two-hole–one-particle (2 h–1p) electronic configurations, which are treated consistently through third and first order in the correlation potential, respectively, by virtue of the ADC(3) secular equations. Compared with experiment, the accuracy of ADC(3) one-electron ionization energies is typically around 0.2 eV, provided a suitably large enough basis set is used.

At high enough electron impact energies ($E_0 > 1.6$ keV, according to the most recent studies on this issue), and considering that a non-coplanar symmetrical experimental set-up is used, which favours clean knocked-down (e, 2e) collision processes characterized by a high electronic momentum transfer and a negligible kinetic energy transfer to the residual cation, it is reasonable to assume that the Born (sudden or vertical), binary encounter and plane wave impulse approximations (PWIA) are valid. Therefore, the triple differential EMS cross-sections for randomly oriented molecules are given by

$$\sigma_{\mathrm{EMS}} \propto \int \mathrm{d}\Omega \left| \left\langle \nu_{\vec{p}} \Psi_f^{N-1} \middle| \Psi_i^N \right\rangle \right|^2, \quad (2)$$

where $\nu_{\vec{p}}$ represents a plane wavefunction $\mathrm{e}^{\mathrm{i}\vec{p}\cdot\vec{r}}$. Under the target Kohn–Sham approximation (TKSA) [36, 37], upon accounting for the dispersion of the ionization intensity over satellites, equation (2) reduces to

$$\sigma_{\mathrm{EMS}} \propto S_i^f \int \mathrm{d}\Omega |\psi_i(\vec{p})|^2, \quad (3)$$

where $\psi_i(\vec{p})$ represents the momentum-space representation, i.e. Fourier transform, of a canonical HF or KS orbital, and S_i^f denotes the associated spectroscopic strength, which accounts for the dispersion of the ionization intensity into shake-up and shake-off processes due to configuration interactions in the final state. With this empirical formula, ground-state electronic correlation is also taken into account through the interplay of the employed exchange-correlation potential [36]. In a first analysis of electron momentum distributions that relate to valence one-electron ionization bands, it is reasonable to assume in a first step that spectroscopic strengths are constant and close to 1. In the framework of one-particle Green's function theory [18] or electron propagator theory [19], these spectroscopic strengths are accounted for through the interplay of Dyson orbitals [19, 24, 29], defined as partial overlaps between the final $\left(\Psi_f^{N-1}\right)$ and initial $\left(\Psi_i^N\right)$ states in equation (2).

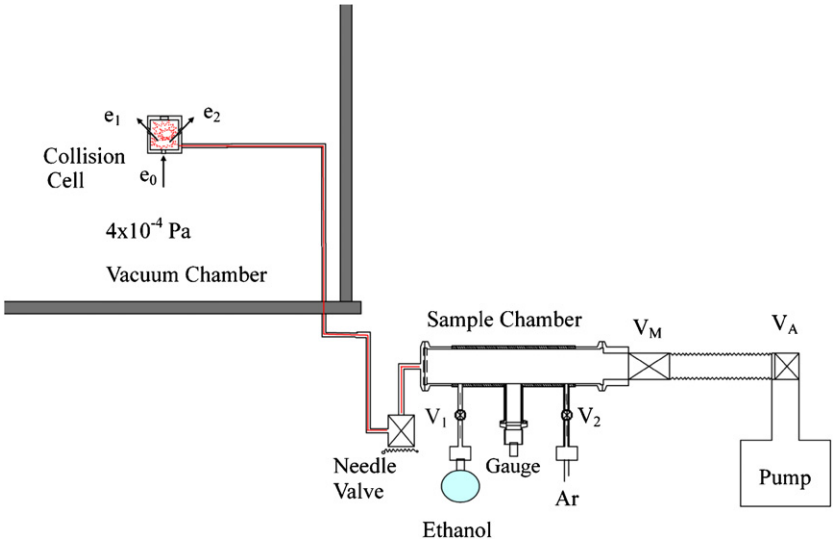

Figure 1. Experimental set-up for gas injection and expansion into the collision chamber.

For a conformationally versatile molecule, the relative abundance f_s of the conformation s at a temperature T can be estimated according to a Boltzmann distribution, that is

$$f_s = g_s \, \mathrm{e}^{-\frac{\Delta G_s}{kT}}, \tag{4}$$

where k is the Boltzmann constant, and g_s is the statistical weight (symmetry number), which is equal to 2 and 1 for the *gauche* and *anti* conformers, respectively. According to thermostatistical calculations of Gibb's free energy differences (ΔG_S) beyond the rigid-rotor harmonic oscillator (RRHO) approximation, the equilibrium mixture characterizing ethanol at room temperature ($T = 298$ K) consists of a major *gauche* fraction (60.7%) and a minor *anti* fraction (39.3%). These thermo-statistical calculations [38] are based on highly accurate estimates of the energy difference between the two conformers, assuming that both species lie in their (electronic, vibrational and rotational) energy ground states.

The calculations discussed in the present work have been performed using density functional theory (DFT) along with the standard hybrid B3LYP functional [39] and with the aug-cc-pVTZ basis set, by means of the Gaussian03 program [40]. The calculation of electron momentum distribution implies Fourier transforms and spherical averaging over all molecular orientations in the gas phase (see chapters 3 and 6 in [16]). Prior to Fourier transforms, Cartesian basis functions have to be projected onto spherical (Slater or Gaussian) basis functions. The newly developed NEMS program [41] which is used to compute spherically averaged electron momentum distributions makes use of general analytic formula [42] for handling in a generic way the atomic basis functions, no matter what is their quantum number for the angular momentum. This program also incorporates an efficient algorithm employing continuous fractions [43] which enables us to overcome the numerical difficulties and convergence problems that most commonly arise at $x \sim 0$ and $x \gg 1$ when computing high-order spherical Bessel functions $j_l(x)$, without any limitation on the associated angular momentum, and which permits therefore treatments of basis sets incorporating formally any type (s, p, d, f, g, h, i, ...) of AO functions. Therefore, with this newly developed program, momentum distributions can be calculated near the limit of completeness for the basis set.

The EMS spectrometer which has been developed at Tsinghua University [44, 45] employs a symmetric non-coplanar kinematical set-up, a double toroidal energy analyser and position sensitive detectors to achieve the energy and angle multi-channel detections. The pressure in the main vacuum chamber (figure 1) is around 4×10^{-4} Pa, which implies an estimated mean free path for the outgoing electrons of $\sim$100 m. The fly distance from the collision point to the electron detectors is only about 0.3 m, so the possibility of secondary collisions can be neglected. The length of the gas tube connecting the needle valve to the collision cell through the vacuum chamber is about 1m (figure 1) and the pressure in the collision cell is about 10^{-2} Pa. This cell has a diameter of $\sim$8 mm. Note that, in contrast with experiments based on free expansions in supersonic jets, the relatively high pressure in the collision cell ensures a full randomization of molecular motions, and thermal equilibrium therefore with the environment. It is also important to note that, because of the extremely limited enthalpy (+0.51 kJ mol^{-1}) and entropy (-0.48 J mol^{-1} K^{-1}) differences between the C_1 and C_s species, the conformer abundances are merely insensitive to the temperature and are not significantly affected therefore by cooling effects, down to 173 K [38].

Significant modifications have been recently implemented on our spectrometer to achieve higher resolutions [46]. Briefly, an electron gun equipped with an oxide cathode, which works at a much lower temperature than the generic filament cathodes, is used to generate the electron beam with a low energy spread and a low divergence angle. The electron beam size is constrained to 0.3 mm in diameter by a molybdenum aperture. The energy resolution varies inversely to the passing energy, i.e. the energy of the electrons when they pass through the energy analyser. This parameter has been adjusted to 50 eV by using a retarding lens. The final experimental energy resolution is mainly limited by the energy spread of the electron beam generated by the electron gun, not by the analyser. The energy resolution could be improved by replacing the

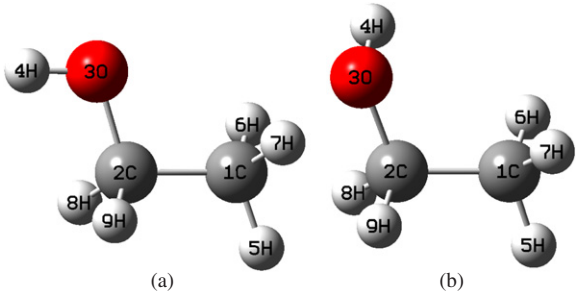

Figure 2. Geometrical structures of the *anti* (left, C_s symmetry) and *gauche* (right, C_1 symmetry) conformers of ethanol.

oxide cathode, and by adjusting the mount precision and the space charge effects. According to a calibration experiment employing Argon, the energy resolution that could be achieved in the present study is $\Delta E = 0.68$ eV (FWHM).

3. Results and discussion

The geometrical structure of the two conformers of ethanol (figure 2) has been optimized at the B3LYP/aug-cc-pVTZ level, using as starting inputs the experimental geometries. The *anti* conformation (figure 2(a)) corresponds to a dihedral HOCC angle of 180° while the *gauche* conformation (figure 2(b)) has a dihedral angle of 61.7°. The *anti* conformation has C_s symmetry, and its electronic ground state has the following core and valence shell configurations:

- $\{(1a')^2\,(2a')^2\,(3a')^2\}$;
- $\{(4a')^2\,(5a')^2\,(6a')^2\,(7a')^2\,(1a'')^2\,(8a')^2\,(9a')^2\,(2a'')^2\,(10a')^2\,(3a'')^2\}$;

respectively. Similarly, the *gauche* form of ethanol belongs to the C_1 point group, and the core and valence shell configurations for its electronic ground state are:

- $\{(1a)^2(2a)^2(3a)^2\}$;
- $\{(4a)^2(5a)^2(6a)^2(7a)^2(8a)^2(9a)^2(10a)^2(11a)^2(12a)^2(13a)^2\}$.

3.1. Binding energy spectra of ethanol

Experimental (e, 2e) ionization spectra are compared in figure 3 with a thermostatistical average of the ADC(3) ionization spectra of the *gauche* (C_1) and *anti* (C_s) conformers of ethanol. The ionization spectra are simulated from the computed ionization energies and spectroscopic (pole) strengths, using as convolution function a Gaussian with a constant full width at half the maximum (FWHM) parameter of 0.8 eV which accounts for the natural line widths and the experimental resolution of the spectrometer (vibrational broadening was neglected). The selected electron binding energies range from 7 eV to 37 eV at an electron impact energy (E_0) of 1200 eV plus electron binding energies (ε_b). Further EMS measurements at $E_0 = 2400$ eV + ε_b were also conducted in order to assess the validity of the plane wave impulse approximation (PWIA) throughout the inner- and outer-valence regions. The spectra displayed in figure 3 were obtained by integrating the (e, 2e) measurements over all azimuthal angles. It can be seen that the peak defining the highest occupied molecular orbital (HOMO, peak 1) is nicely resolved and exhibit very limited overlap with other states.

The (e, 2e) ionization spectra were fitted onto Gaussian functions, in order to infer from the angular analysis embodied in equation (1) the experimental electron momentum distributions characterizing each resolvable set of orbitals.

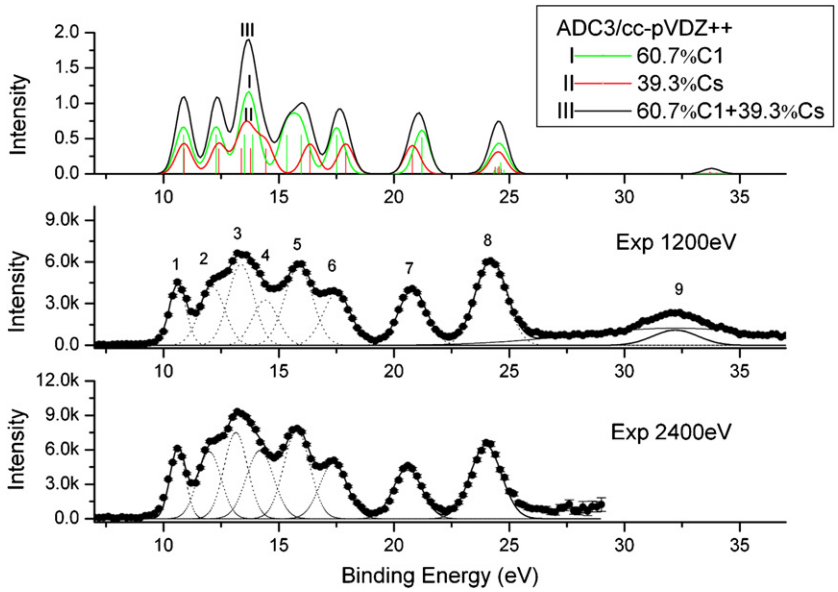

Figure 3. Comparison of the thermally averaged ADC(3)/cc-pVDZ++ ionization spectrum of ethanol and of the individual conformer components (top) with EMS electron binding energy spectra at electron impact energies of 1200 eV (+ electron binding energy, ε_b, middle) or 2400 eV + ε_b (bottom). The experimental spectra displayed in this figure were summed over all ϕ angles. Experimental intensities are given as electron counts, and k (kilo) refers to a scale factor 1000.

Table 1. Ionization energies of ethanol (in eV). EMS and ADC(3) pole strengths are given in brackets.

Orbital	PES(HeII)[a]	EMS[b]	ADC(3)/cc-pVDZ++ *anti* (C_s)	ADC(3)/cc-pVDZ++ *gauche* (C_1)
MO13	10.7	10.6(1.0)	10.887 (3a″)(0.913)	10.861 (13a)(0.911)
MO12	12.1	12.1(1.0)	12.392 (10a′)(0.914)	12.279 (12a)(0.916)
MO11	13.3	13.4(1.0)	13.372 (2a″)(0.915)	13.513 (11a)(0.915)
MO10	*13.9*	–	*13.77 (9a′)(0.915)*	*13.865 (10a)(0.912)*
MO9	*(14.5)*	*14.4(1.0)*	*14.431 (8a′)(0.907)*	–
MO9	*(15.0)*[c]	–	–	*15.343 (9a)(0.905)*
MO8	16.0	15.9(1.0)	16.534 (1a″)(0.901)	15.973 (8a)(0.906)
MO7	17.4	17.5(1.0)	17.901 (7a′)(0.901)	17.508 (7a)(0.9)
MO6	20.7	20.8(0.90)	20.8 (6a′)(0.849)	21.204 (6a)(0.848)
MO5	24.2	24.2(0.64)	5a′	5a
			24.386 (0.248)	23.862(0.029)
			24.549(0.266)	24.334(0.048)
			24.639(0.182)	24.346 (0.082)
				24.477(0.135)
				24.599(0.024)
				24.632(0.263)
				24.767(0.092)
MO4		32.2(0.1)	4a′	
			33.661(0.021)	
			33.7 (0.072)	
			33.757(0.039)	
			33.991(0.041)	

[a] See [15].
[b] In our rescaling of experimental intensities, we assume that the pole strengths of the outer-valence orbitals are equal to 1.
[c] Our assignment (see also [38]).

In this analysis, use was made of the ADC(3) vertical ionization potentials presented in table 1 for assigning these bands and calculating the corresponding electron momentum distributions, and of Franck–Condon widths, as estimated from photoelectron spectroscopy (PES) measurements [14, 15]. More specifically, the centres of the Gaussian bands used to deconvolve the experimental spectra were estimated based on the position of the peaks seen in PES measurements with small adjustments in order to compensate the asymmetries in the shape of the Franck–Condon envelopes. These distributions were also folded with the EMS instrument energy resolution of 0.68 eV (FWHM). One of these Gaussian bands (identified as band 4) was necessary for reproducing a shoulder at 14.4 eV in the (e, 2e) ionization spectra, which can be merely ascribed (table 1) to the 8a′ orbital (MO9) of the anti (C_s) conformer and its associated vibrational tail. In view of the ADC(3) simulations displayed in figure 3 (see also [38]), the 9a orbital of the *gauche* (C_1) conformer is then ascribed (table 1) to band 5. Two Gaussian functions were also used to fit the much broader experimental intensity distribution around 32.2 eV (band 9). The exceedingly large band width characterizing this band is consistent with a particularly strong breakdown of the orbital picture of ionization in the theoretical ADC(3) spectra, and indicative of a decay of shake-up states associated with the O_{2s} orbital through the ionization of a second electron into the continuum (the vertical double ionization threshold of ethanol is indeed around ∼29.9 eV, according to CCSD(T)/aug-cc-pVTZ computations [38]).

ADC(3) estimates of the valence one-electron and shake-up ionization energies can be compared in table 1 with the available experimental data. The employed basis set is the standard Dunning's cc-pVDZ basis set, supplemented by *s* and *p* diffuse functions on the C, O and H atoms, and referred therefore to as the cc-pVDZ++ basis set [31, 32]. Remarkable differences can be noted between the ionization energies of the MOs 7, 8 and 9 of the *anti* and *gauche* conformers, yielding a rather strong conformational fingerprint at ∼14.4 eV for the *anti* species in the ionization spectrum (figure 2, top), due to a stabilization by 0.9 eV of MO9 in this conformer [38] compared with the *gauche* conformer.

Prior to proceeding further with our analysis of the electronic wavefunction of ethanol and its interplay with the molecular conformation, it must be mentioned at this stage that all the momentum distributions that are provided in the following were subject to a global rescaling of the experimental intensities at electron binding energies ranging from 8 eV to 19 eV (i.e. peaks 1 to 6 in figure 2) onto the theoretical intensities ascribed to MOs 7–13, using normalized ADC(3) Dyson orbital electron momentum distributions as reference. More specifically, the experimental intensities have been multiplied by a common rescaling factor obtained through a fit of the total momentum distribution inferred from peaks 1–6 in figure 2 onto the sum of the spherically and thermally averaged, resolution folded momentum densities associated with MOs 7–13, respectively, under the constraint that each of these theoretical momentum densities remains normalized. The motivations for this choice stem from the fact that the momentum distributions characterizing these orbitals remain free of shake-up contamination [37] and display almost constant spectroscopic strengths (table 1), varying from 0.913 to 0.901 according to the ADC(3) results obtained for the eight outermost orbitals (MOs 7–13). The obtained rescaling

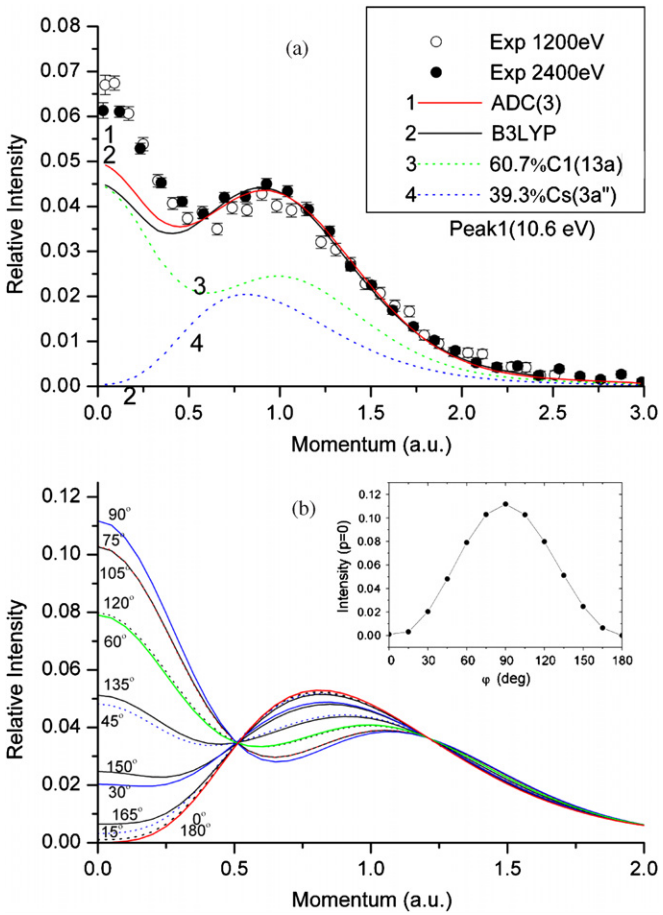

Figure 4. (a) Comparison of the experimental momentum distribution characterizing band 1 with convolved, thermally and spherically averaged momentum distributions of the highest occupied molecular orbital (HOMO) of ethanol at an impact energy of 1200 eV + ε_b and 2400 eV + ε_b (the individual contributions in curves 3 and 4 are B3LYP/aug-cc-pVTZ results); (b) evolution of the spherically averaged momentum distributions characterizing the HOMO of ethanol as a function of the C_1–C_2–O_3–H_4 torsion angle (φ) describing the internal rotation of the hydroxyl group (B3LYP/aug-cc-pVTZ results). The inset illustrates correspondingly the evolution of the (e, 2e) ionization intensity at $p = 0$.

constant was then used to experimentally evaluate the pole strengths characterizing the inner-valence ionization lines.

3.2. The highest occupied molecular orbital (HOMO)

We compare in figure 4 the experimentally apparent momentum distribution for the highest occupied molecular orbital (HOMO) at electron impact energies of 1200 eV and 2400 eV with thermally and spherically averaged simulations at room temperature. The theoretical orbital momentum distributions have been convolved with the experimental momentum resolution at $E_0 = 1200$ eV + ε_b using a Monte Carlo method [47]. The achieved momentum resolutions are $\Delta p \sim 0.16$ au (FWHM) or $\Delta p \sim 0.069$ au (standard deviation) at an impact energy (E_0) of 1200 eV (+ε_b). The electron density of the HOMO of the C_s species is dominated by the lone electron pair of the O_{2p} and H_{1s} orbitals, which yields the bump located at $p = 1$ au in the orbital momentum distributions.

A rather strong discrepancy between theory and experiment is immediately apparent in the low momentum region ($p < 0.5$ au) of the HOMO (figure 4(a)), in the form of a very strong underestimation of experimentally recorded (e, 2e) ionization cross-sections by a simple thermal average of the contributions of the two conformers. Since the observed momentum distribution is seemingly much closer to that of the HOMO of the *gauche* conformer (curve 3), one may be tempted to resolve this discrepancy by increasing the abundance of the *gauche* conformer: an almost perfect agreement with experiment is indeed amenable through a least-squares fitting of the experimental curve against the simulations, but this would yield a questionable *gauche*/*anti* ratio of 80/20. Note that the *gauche* and *anti* conformers are almost isoenergetic according to available high-resolution spectroscopic measurements [2, 4–10] and high-level calculations at the confines of relativistic quantum mechanics [2, 11]. Therefore, their relative abundances are almost independent of the temperature [38], and an increase of the abundance of the *gauche* conformer to ∼80% cannot be explained on simple thermodynamical grounds. Such an increase would furthermore lead to stronger discrepancies between the theoretical and experimental momentum distribution of all other outer-valence orbitals. In view of the similarity of the 3a″ (HOMO) orbital of the C_s conformer with a *d*-type atomic orbital, and in analogy with recent works on the electron momentum distributions of diatomic oxygen [48] or ethylene [49], it is natural in a next step to wonder whether the particularly strong discrepancies that are observed between theory and experiment for the HOMO can be ascribed to distorted wave effects, i.e. to a breakdown of the plane wave impulse approximation [50–52]. The EMS measurements that are presented in figure 4(a) at much higher electron impact energies ($E_0 =$ 2.4 keV) indicate that that the plane wave impulse approximation (PWIA) employed in the simulation is still a good and a very valid approximation at $E_0 = 1.2$ keV. In our opinion, the most likely explanation for this discrepancy must be sought into a more pronounced conformational disorder, because of the extreme flatness of the potential energy curve characterizing the OH rotation in ethanol and very likely departures therefore from equilibrium structures defining energy minima, due to thermally induced internal motions. Indeed, the *gauche–anti* OH torsional energy barrier in ethanol does not exceed 364.3 cm^{-1} [8] according to IR spectroscopic measurements.

In line with this observation, we analyse in figures 4(b) and 5 the evolution of the electron density contours of the HOMO in configuration (r) space and the associated momentum distributions of the HOMO as a function of the C–C–O–H torsion angle (φ). Figure 5 indicates that the mirror anti-symmetry of the electron density for the HOMO when $\varphi =$ 180° (*anti* conformer) progressively breaks as the hydroxyl group rotates, yielding correspondingly a reversal of the *p*-type MD profile characterizing the HOMO of the C_s conformer into a mixed *s*–*p* type profile (figure 4(b)). The electron density around the C_2–H_8 and C_2–H_9 bonds reduces upon the hydroxyl rotation, and almost disappears at $\varphi = 90°$, while the

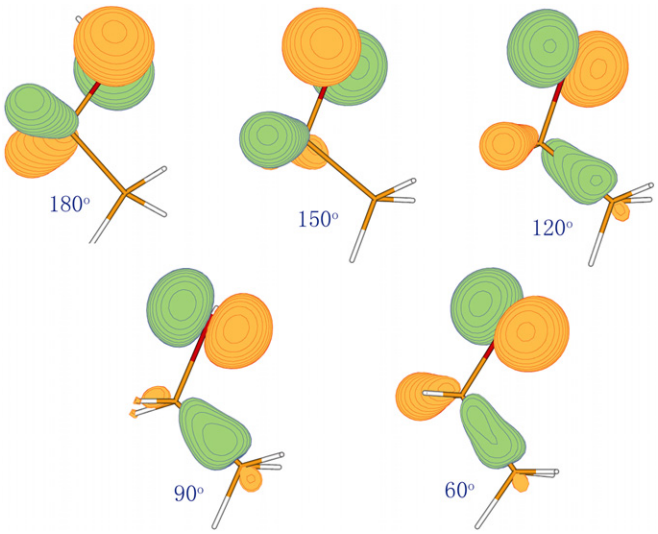

Figure 5. Evolution of the contour plots of the HOMO of ethanol as a function of the C_1–C_2–O_3–H_4 torsion angle describing the internal rotation of the hydroxyl group around the C–C bond. The displayed molecular orbitals were drawn using Molden 4.3 [53] and a contour value of 0.05 (B3LYP/aug-cc-pVTZ results).

electron density around the C_2–C_1 bond increases gradually, and reaches correspondingly a maximum at $\varphi = 90^\circ$. These alterations of the molecular orbital topology are the rather obvious consequence of anomeric (through space) and bonding (in phase) interactions [31] between the oxygen lone pairs and the vicinal C–C bond.

Figure 4(b) indicates that the most important orbital distortions induced by the internal rotation of the hydroxyl groups dominate the orbital electron distributions in the long range, which is in line with the release of symmetry constraints. When $\varphi < 90^\circ$, the momentum distributions of the HOMOs at low electron momenta ($p < 0.50$) decrease as φ increases; in contrast, when $\varphi > 90^\circ$, the opposite trend prevails within this range of electron momenta. In other words, the maximum in (e, 2e) ionization intensity characterizing band I at a zero electron momentum is reached when $\varphi = 90^\circ$ (see inset of figure 4(b)). It seems thus quite likely that the larger experimental (e, 2e) ionization cross-sections characterizing the HOMO at $p = 0$ are due to the contribution of non-equilibrium molecular structures around the energy barrier separating the *gauche* and *anti* conformers. Since the methyl and hydroxyl rotations are strongly coupled [2], large-scale molecular dynamical simulations employing accurate enough force fields would be necessary to quantitatively assess the outcome of thermal motions and departures from a simple thermostatistical depiction focusing on energy minima only.

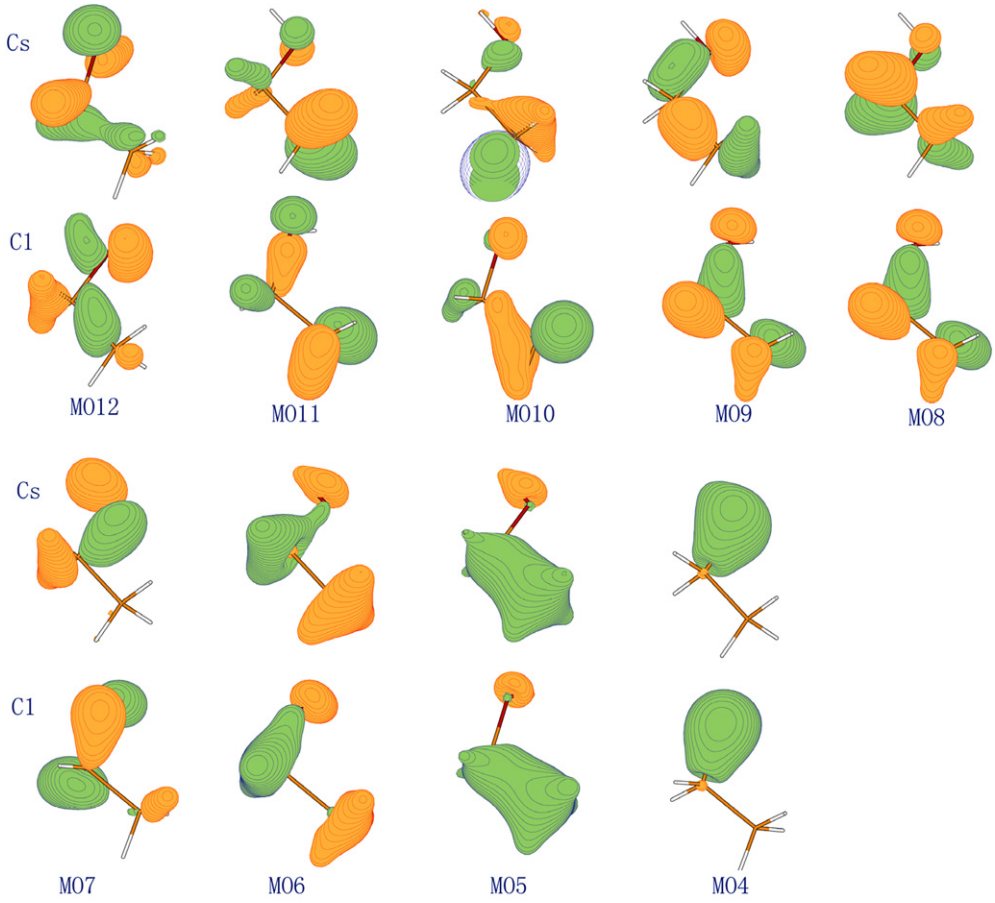

Figure 6. Contour plots of all valence orbitals of the two conformers of ethanol, using Molden 4.3 [53] and a contour value of 0.05 (B3LYP/aug-cc-pVTZ results).

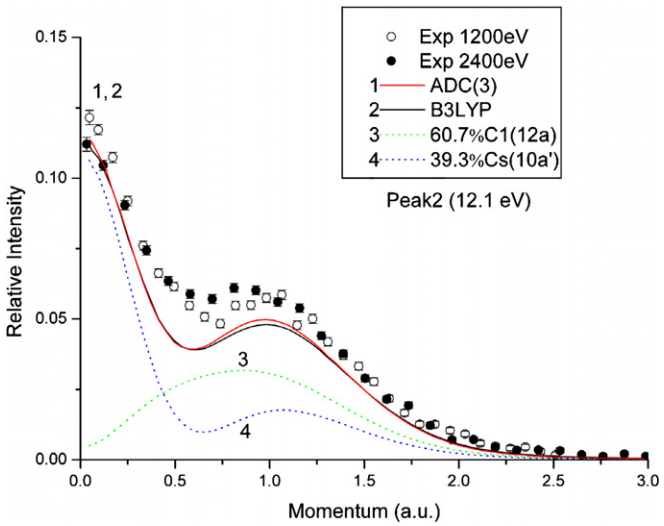

Figure 7. Comparison of the experimental momentum distribution characterizing band 2 with convolved, thermally and spherically averaged momentum distributions of the HOMO-1 orbital of ethanol at an impact energy of 1200 eV + ε_b and 2400 eV + ε_b. The individual conformer contributions are given at the B3LYP/aug-cc-pVTZ level (curves 3, 4).

3.3. Other orbitals

In figure 6, we compare contour plots for the valence orbitals of the *anti* (C_s) and *gauche* (C_1) conformers. It is interesting to note that these contours strongly vary from one conformer to the other. Significant differences are also seen therefore in the momentum distributions. Figure 7 compares the experimental momentum distributions of MO12 (HOMO−1) with theoretical calculations. The calculated momentum distributions of the *gauche* conformer (12a, curve 3) are significantly different from that of the *anti* conformer (10a′, curve 4). Orbital 10a′ exhibits a momentum distribution of mixed *s–p* type, which is characterized therefore by a maximum in intensity at $p = 0$, and by the presence of a shallow bump at $p = 1.2$ au. In contrast, orbital 12a from the C_1 conformer yields a *p*-type momentum distribution, characterized by vanishingly small (e, 2e) ionization intensities at $p = 0$, and a maximum at $p = 0.9$ au. The simulations based on a Boltzmann statistical averaging of the conformer abundances (curve 1, curve 2) reproduce well this time the experimental momentum distributions. This excellent agreement between the experimental momentum distributions and the theoretical simulations prevents us to attempt to eliminate the discrepancy in figure 4(a) by adjusting the conformer weights, regardless of thermodynamical considerations.

The closely spaced one-electron ionization lines originating from MO8–MO11 result in rather significant overlaps of the Gaussian bands 3, 4 and 5 in the EMS ionization spectra (figure 3). Because of the strong influence of the molecular conformation upon ionization energies [38], it is essential to rely on accurate ionization energies such as ADC(3) data for correctly unravelling the associated momentum distributions. The contributions of the Gaussian bands 3 and 4 to the EMS ionization spectra cannot be

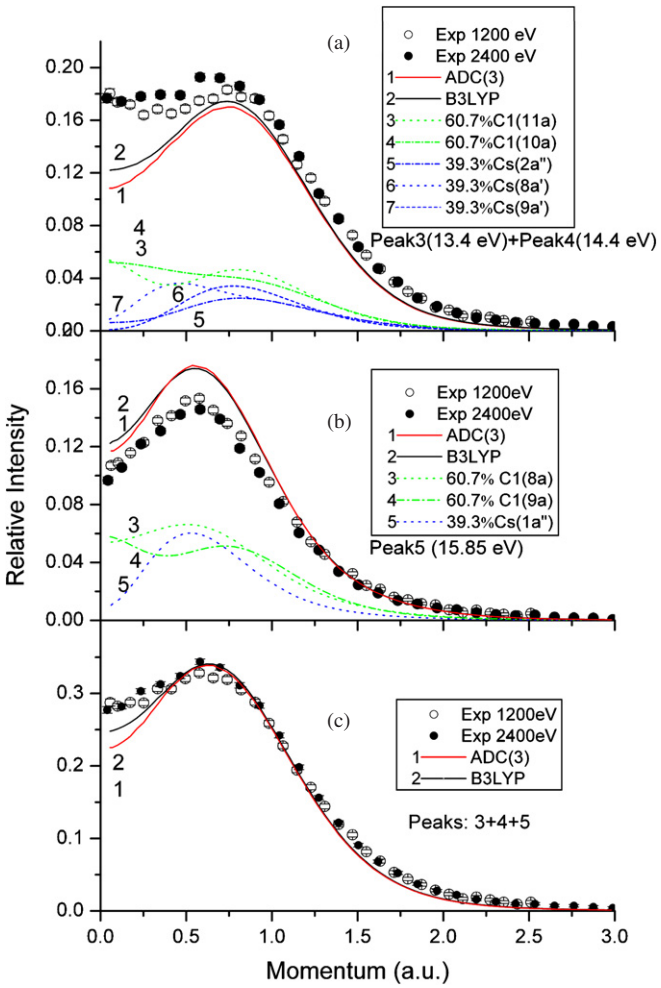

Figure 8. Comparison of the experimental momentum distribution characterizing bands 3–5 at electron impact energies of 1200 eV + ε_b and 2400 eV + ε_b with convolved, thermally and spherically averaged electron momentum distributions for model sets of one-electron ionization lines. The individual orbital contributions (see insets for details) are provided at the B3LYP/aug-cc-pVTZ level.

disentangled in a physically meaningful way, because of the too limited energy interval separating these two bands (1.0 eV), as well as the too-limited intensity of band 4, which essentially relates to the one-electron ionization line produced by the 8a′ (MO9) orbital of the C_s conformer, and which effectively emerges as a rather poorly defined shoulder in the experimental spectrum (figure 3).

We therefore compare in figure 8(a) the summed momentum distributions for these two bands with that characterizing a set of orbitals comprising the 10a and 11a orbitals (MOs 10 and 11) of the *gauche* (C_1) conformer, and the 2a″, 8a′, 9a′ orbitals (MO's 9, 10, 11) of the *anti* (C_s) conformer. Correspondingly, the momentum distributions characterizing band 5 is analysed (figure 8(b)) in terms of contributions of the 8a and 9a orbitals (MO's 8 and 9) of the C_1 conformer, and of the 1a″ orbital (MO8) of the C_s conformer. In view of the intricacy of the spectral bands associated with these orbitals, the agreement between theory and experiment is fair, and qualitatively corroborates the

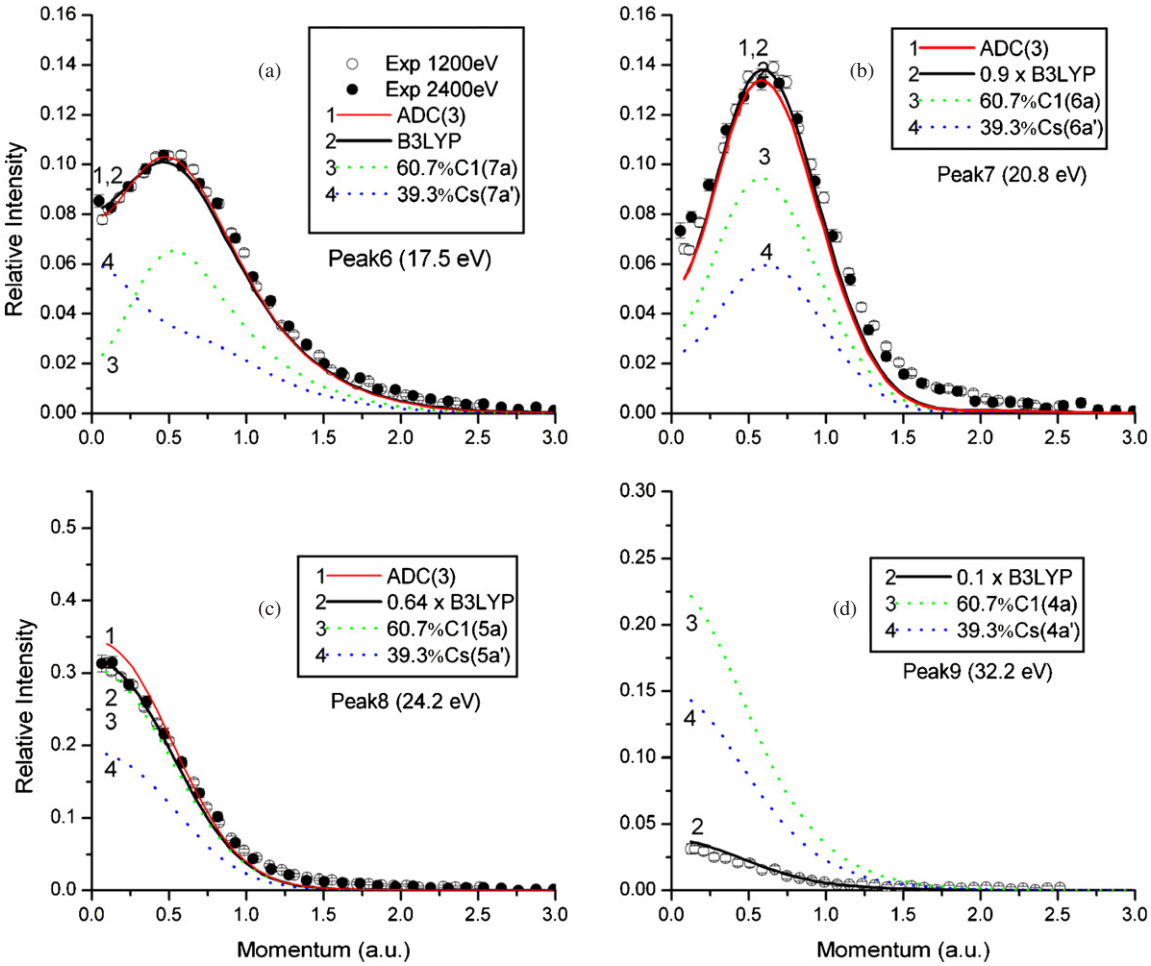

Figure 9. Comparison of the experimental momentum distribution characterizing bands 6–9 at electron impact energies of 1200 eV + ε_b and 2400 eV + ε_b with convolved, thermally and spherically averaged electron momentum distributions for model sets of one-electron (figure 9(a) or (b)) or shake-up (figure 9(c) or (d)) ionization lines. The (normalized) individual orbital contributions (see insets for details) were rescaled onto the corresponding conformer abundances (B3LYP/aug-cc-pVTZ results).

ADC(3) assignment. Again, changing the electron impact energy has almost no physically significant influence on the experimentally obtained momentum distributions, and we may presume therefore that the plane wave impulse approximation is valid. A very satisfactory match between theory and experiment is obtained (figure 8(c)) when comparing summed momentum distributions for MOs 8–11 and for bands 3–5 in the EMS ionization spectrum, indicating that the discrepancies that are seen for the underlying components (3 + 4 and 5) are merely the result of overlap effects.

In figures 9(a) and (b), we compare the experimental momentum distributions characterizing bands 6 and 7 with theoretical simulations for the innermost outer-valence [O_{2p}+C_{2p}+H_{1s}] orbital (MO7) and for the outermost [C_{2s}] inner-valence orbital (MO6), respectively. These orbitals are well isolated from all other orbitals, they are not subject to a particularly pronounced breakdown of the orbital picture of ionization, and their energy exhibits very little dependence on the molecular conformation [38]. For these two orbitals, the match between the calculated and experimentally inferred momentum densities is simply perfect. Note that, compared with the one-electron ionization lines associated with MO 7–13, the measurements indicate a decrease of the experimentally inferred spectroscopic strength of MO6 by ∼10%, to compare with a drop of ADC(3) pole strengths from ∼0.91 to ∼0.85. MO6 merely describes an anti-bonding combination of C_{2s} atomic orbitals centred on the C_1 and C_2 atoms, and exhibits only one curved nodal surface in the dominant conformer (C_1), which explains the resemblance of its momentum distribution with a *p*-type profile.

Proceeding further with band 8 at 24.2 eV (figure 9(c)), we note this time at the ADC(3) level a severe breakdown of the orbital picture of ionization, in the form of a dispersion of the ionization intensity over several C_{2s} shake-up states of comparable strengths (table 1, figure 3). A perfect match between theory and experiment is obtained at the ADC(3) level upon summing the contributions from all identified shake-up states in this energy region, whereas the associated Kohn–Sham momentum distribution has to be rescaled by a factor equal to 0.64. This value empirically defines the empirical spectroscopic strength characterizing band 8, and can be compared with total ADC(3) pole strengths around 0.70 and 0.67 for the 5a′ and 5a orbitals of the C_s and C_1 conformers, respectively. Beyond the double ionization threshold at 29 eV,

the breakdown of the orbital picture of ionization intensifies at the ADC(3) level (table 1, figure 2) by virtue of a dispersion of the ionization intensity over many more states defining discrete approximations to resonances in the energy continuum (shake-off states). Unsurprisingly therefore, a rescaling of the B3LYP Kohn–Sham momentum distribution (figure 9(d)) for the O_{2s} band (9) at 32.2 eV yields an extremely low value for the experimental spectroscopic strength (0.1). Despite these many-body complications, the O_{2s} and lowest C_{2s} ionization bands at 32.2 and 24.2 eV associated with MOs 4 and 5 are unambiguously of the *s*-type (figures 9(c) and (d)), which is in line with the idea that each state or energy resonance above the shake-up and shake-off onsets borrows its ionization intensity to one specific orbital.

4. Conclusions

The valence electronic structure and momentum-space electron density distributions of ethanol have been investigated with our recently developed high-resolution electron momentum spectrometer. The measurements are compared to Boltzmann-weighted simulations for the two known conformers (C_s, C_1) based on Kohn–Sham (B3LYP) orbital densities, as well as high-level [ADC(3)] one-particle Green's function calculations of one-electron and shake-up ionization energies and the related spectroscopic strengths and Dyson orbital densities. Temperature effects are accounted for by averaging the contributions of the two conformer species to spectral bands and momentum distributions in an analysis based on Boltztman's statistical thermodynamics. It was found that both the one-electron binding energies and electron momentum distributions strongly depend on the molecular conformation. In particular, the momentum distribution of the highest occupied molecular orbital (HOMO) is extremely sensitive to an internal rotation of the hydroxyl group. The present study therefore nicely confirms the view [28] that electron momentum spectroscopy can be used as a very powerful probe of the molecular conformation and of its interplay with the underlying electronic structure. In this study, rather significant discrepancies between the experimentally obtained momentum distributions for this orbital and simulations based on a thermo-statistical average of the respective contributions of the two prevailing conformers can be tentatively ascribed to a strong structural disorder in the gas phase. In view of the characteristics of our experimental set-up for gas expansion into a confined collision chamber, which favours thermal equilibration with the environment, and considering the extremely limited time that is required for the inter-conversion of the C_1 and C_s species ($\sim 10^{-12}$ s) over an energy barrier of 400 cm^{-1} only, it seems highly unlikely that the discrepancies that were observed for the outermost ionization bands between the calculated and experimentally inferred momentum distributions are the results of non-equilibrium dynamics in the gas phase. Furthermore, the experimental momentum distributions are merely insensitive to an increase of the electron impact energy from 1.2 keV to 2.4 keV. The observed discrepancies between theory and experiment thus cannot be due to a particularly strong breakdown of the plane wave impulse approximation, but are rather indicative of significant departures of the molecular structure from energy minima due to large-amplitude and thermally induced motions. Further studies employing molecular dynamics will be needed for assessing this issue.

Acknowledgments

This work is supported by the National Natural Science Foundation of China under contract nos 10575062 and 10704046, and by the Specialized Research Fund for the Doctoral Program of Higher Education under 20050003084. On the Belgian side, the authors acknowledge financial support from the FWO-Vlaanderen, the Flemish branch of the Belgian National Science Foundation, and from the BijzonderOnderzoeksFonds (BOF: special research fund) of Hasselt University. BH is especially grateful to the scientific research network 'Density Functional Theory: Fundamental and Applied Aspects' sponsored by the FWO-Vlaanderen (Belgium) for a one-year visiting post-doctoral fellowship at Hasselt University.

References

[1] Schriver A, Schriver-Mazzuoli L, Ehrenfreund P and d'Hendecourt L 2007 *Chem. Phys.* **334** 128
[2] Senent M L, Smeyers Y G, Domingues-Gómez R and Villa M 2000 *J. Chem. Phys.* **112** 5809
[3] March J 1985 *Advanced Organic Chemistry, Reactions, Mechanisms, and Structures* 3rd edn (New York: Wiley)
[4] Pearson J C, Sarsty K V L N, Herbst E and de Lucia F C 1996 *J. Mol. Spectrosc.* **175** 146
[5] Coussan S, Bouteiller Y, Perchard J P and Zheng W Q 1998 *J. Phys. Chem.* A **102** 5789
[6] Barnes A J and Hallam H E 1970 *Trans. Faraday Soc.* **66** 1932
[7] Ehbrecht M and Huisken F 1997 *J. Phys. Chem.* A **101** 7768
[8] Durig J R and Larssen R A 1989 *J. Mol. Struct.* **238** 195
[9] Abu-samha M and Børve K J 2006 *Phys. Rev.* A **74** 042508
[10] Abu-samha M, Børve K J, Sæthre L J and Thomas T D 2005 *Phys. Rev. Lett.* **95** 103002
[11] Kahn K and Bruice T C 2005 *Chem. Phys. Chem.* **6** 487
[12] Salam A and Deleuze M S 2002 *J. Chem. Phys.* **116** 1296
[13] Deleuze M S, Claes L, Kryachko E S and François J P 2003 *J. Chem. Phys.* **119** 3106
[14] Kimura K, Katsuwata S, Achiba Y, Yamazaki T and Iwata S 1981 *Handbook of HeI Photoelectron Spectra of Fundamental Organic Molecules* (New York: Halsted)
[15] Potts A W, Williams T A and Price W C 1972 *J. Chem. Soc. Faraday Discuss.* **54** 104
[16] Weigold E and McCarthy I E 1999 *Electron Momentum Spectroscopy* (New York: Kluwer)
[17] Brion C E 1986 *Int. J. Quantum Chem.* **29** 1397
[18] Cederbaum L S and Domcke W 1977 *Adv. Chem. Phys.* **36** 205
[19] Öhrn Y and Born G 1981 *Adv. Quantum Chem.* **13** 1
[20] Ning C G, Ren X G, Deng J K, Zhang S F, Su G L, Huang F and Li G 2005 *J. Chem. Phys.* **122** 224302
[21] Takahashi M, Watanabe N, Khajuria Y, Udagaw Y and Eland J H D 2005 *Phys. Rev. Lett.* **94** 213202
[22] Shan X, Chen X J, Zhou L X, Li Z J, Liu T, Xue X X and Xu K Z 2006 *J. Chem. Phys.* **125** 154307
[23] Ning C G, Ren X G, Deng J K, Zhang S F, Su G L, Zhou H, Li B, Huang F and Li G Q 2005 *Chem. Phys. Lett.* **402** 175

[24] Ning C G, Ren X G, Deng J K, Su G L, Zhang S F, Knippenberg S and Deleuze M S 2006 *Chem. Phys. Lett.* **421** 52
[25] Huang Y R, Ning C G, Deng J K and Deleuze M S 2008 *Phys. Chem. Chem. Phys.* **10** 2374
[26] Neville J J, Zheng Y and Brion C E 1996 *J. Am. Chem. Soc.* **118** 10533
[27] Neville J J, Zheng Y and Brion C E 1995 *Science* **270** 786
[28] Deleuze M S, Pang W N, Salam A and Shang R C 2001 *J. Am. Chem. Soc.* **123** 4049
[29] Deleuze M S and Knippenberg S 2006 *J. Chem. Phys.* **125** 104309
[30] Yang T C, Su G L, Ning C G, Deng J K, Wang F, Zhang S F, Ren X G and Huang Y R 2007 *J. Phys. Chem.* A **111** 4927
[31] Huang Y R, Knippenberg S, Hajgató B, François J-P, Deng J K and Deleuze M S 2007 *J. Phys. Chem.* A **111** 5879
[32] Knippenberg S, Huang Y R, Hajgató B, François J-P, Deng J K and Deleuze M S 2007 *J. Chem. Phys.* **127** 174306
[33] McCarthy I E and Weigold E 1991 *Rep. Prog. Phys.* **91** 789
[34] Coplan M A, Moore J H and Doering J P 1994 *Rev. Mod. Phys.* **66** 985
[35] Deleuze M S, Giuffreda M G, François J-P and Cederbaum L S 1999 *J. Chem. Phys.* **111** 5851 and references there in
[36] Duffy P, Chong D P, Casida M E and Salahub D R 1994 *Phys. Rev.* A **50** 4704
[37] Zheng Y *et al* 1996 *Chem. Phys.* **212** 269
[38] Morini F, Hajgató B, Deleuze M S, Ning C G and Deng J K 2008 *J. Phys. Chem.* **A** at press
[39] Lee C, Yang W and Parr R G 1988 *Phys. Rev.* B **37** 785
[40] Frisch M J *et al* 2003 *Gaussian03* revision D02 (Pittsburgh, PA: Gaussian)
[41] Ning C G, Hajgató B, Huang Y R, Zhang S F, Liu K, Luo Z H, Knippenberg S, Deng J K and Deleuze M S 2008 *Chem. Phys.* **343** 19
[42] Mathar R J 2002 *Int. J. Quantum Chem.* **90** 227
[43] Lentz W J 1976 *Appl. Opt.* **15** 668
[44] Ren X G, Ning C G, Deng J K, Zhang S F, Su G L, Huang F and Li G Q 2005 *Rev. Sci. Instrum.* **76** 063103
[45] Ning C G, Deng J K, Su G L, Zhou H and Ren X G 2004 *Rev. Sci. Instrum.* **75** 3062
[46] Ning C G, Zhang S F, Deng J K, Liu K, Huang Y R and Luo Z H 2008 *Chin. Phys.* **17** 1674
[47] Duffy P, Casida M E, Brion C E and Chong D P 1992 *Chem. Phys.* **159** 347
[48] Ning C G, Ren X G, Deng J K, Su G L, Zhang S F and Li G Q 2006 *Phys. Rev.* A **73** 022704
[49] Ren X G, Ning C G, Deng J K, Zhang S F, Su G L, Huang F and Li G Q 2005 *Phys. Rev. Lett.* **94** 163201
[50] Brion C E, Zheng Y, Rolke J, Neville J J, McCarthy I E and Wang J 1998 *J. Phys. B: At. Mol. Opt. Phys.* **31** L223
[51] Takahashi M, Saito T, Hiraka J and Udagawa Y 2003 *J. Phys. B: At. Mol. Opt. Phys.* **36** 2539
[52] Ning C G, Ren X G, Deng J K, Zhang S F, Su G L, Huang F and Li G Q 2005 *Chem. Phys. Lett.* **407** 423
[53] Molden was written by Schaftenaar G 1991 CAOS/CAMM Center Nijmegen Toernooiveld, Nijmegen, The Netherlands